www.czasopisma.pan.pl PAN www.journals.pan.pl
Opto-Electronics Review 26 (2018) 81–91

Contents lists available at ScienceDirect

Opto-Electronics Review

journal homepage: http://www.journals.elsevier.com/opto-electronics review

# Electron paramagnetic resonance study of impurities and point defects in oxide crystals

I. Stefaniuk

*Centre for Microelectronics and Nanotechnology, University of Rzeszow, ul. Pigonia 1, 35-959 Rzeszow, Poland*

ARTICLE INFO

*Article history:*
Received 16 January 2017
Received in revised form 31 January 2018
Accepted 19 February 2018
Available online 7 March 2018

*Keywords:*
Electron paramagnetic resonance
Oxide crystals
Point defects
$Mn^{2+}$
$Mn^{4+}$
$Co^{2+}$
$Fe^{3+}$
$Cr^{3+}$
$Nd^{3+}$ and $Er^{3+}$ ions
Optical materials
Spin-Hamiltonian
Superposition model
Spin-lattice relaxation time,

ABSTRACT

In this topic review the results of the X-band electron paramagnetic resonance (EPR) measurements of Mn, Co, Cr, Fe ions in $YAlO_3$ (YAP) crystals and Fe ions in $LiNbO_3$ (LNO) crystals and of chromium doped $Bi_{12}GeO_{20}$ (BGO) and $Ca_4GdO(BO_3)_3$ single crystals, are presented. It is well known that the oxide crystals (for example:YAP, LNO, BGO) are one of the most widely used host materials for different optoelectronic applications. The nature of point defect of impurities and produced in the oxide crystal after irradiation by bismuth ions and after irradiation by the $^{235}U$ ions with energy 9.47 MeV/u and fluency $5 \times 10^{11}$ $cm^{-1}$ is discussed. The latter is important for applications of these oxide crystal as laser materials.



**Contents**



*E-mail address:* istef@ur.edu.pl

https://doi.org/10.1016/j.opelre.2018.02.002
1896-3757/

## 1. Introduction

The oxide crystals (for example: YAP, LNO, BGO) are one of the most widely used host

materials for different optoelectronic applications. The most known use of these crystals are laser materials. In this respect, it is particularly important to know the nature of defects. It is preferred for this purpose to produce artificial defects in the above named materials and to examine them by so precise method which is Electron Paramagnetic Resonance (EPR). It is advantageous to briefly describe some of the most important oxide crystals for approximations' background and formulation of research questions.

Yttrium orthoaluminate crystals ($YAlO_3$ or YAP) are one of the most important materials for solid-state lasers. Recently, some new interesting properties of Mn-doped $YAlO_3$ have been reported, among them strong photochromic effect [1] and intensive thermally stimulated luminescence (TL) after $\gamma$ –irradiation [2]. Manganese ions in $YAlO_3$:Mn crystals as a rule are present in a form of $Mn^{4+}$ ions in the octahedral coordination ($Al^{3+}$ positions) and $Mn^{2+}$ ions in the strongly distorted dodecahedral coordination ($Y^{3+}$ positions) [1,3–6]. Crystals being exposed to a blue-green laser light show an intensive bluish-gray coloration caused by $Mn^{5+}$ ions created as a result of the $Mn^{4+} \rightarrow Mn^{5+} + e^-$ photoionization process [1,3]. In such a way, the $Mn^{4+}$ ions demonstrate sensitivity to the visible light exposure. The $Mn^{2+}$ ions are sensitive to the ionizing radiation such as X- or $\gamma$ –rays, as well as UV radiation [7]. Explanation of this effects is required. Yttrium aluminum perovskite $YAlO_3$ crystals doped with rare-earth ions ($Nd^{3+}$, $Tm^{3+}$, $Er^{3+}$) belong to the most important solid state laser materials [8,9], as well as they are also promising materials for scintillators (YAP:Ce) [10], and as substrates for thin films' epitaxy [11]. Co-doped oxide crystals are attractive materials for 'eye safe' laser operation near 1.5 μm and as nonlinear absorbers for passive Q-switching [11,12]. EPR and optical spectra, as well as nonlinear absorption properties of $Y_3Al_5O_{12}$:Co, $SrLaAlO_4$:Co, $Mg_2Al_2O_4$:Co, $LaGaO_3$:Co, and $SrLaGa_3O_7$:Co were investigated in Refs. 12–16. The EPR spectra of various ions in $YAlO_3$ crystals, e.g. the 3dN ions $Cr^{3+}$, $Ti^{3+}$, $Mn^{4+}$, $Mn^{5+}$ and $Fe^{3+}$ [3,17–20] and the 4fN ions $Er^{3+}$, $Nd^{3+}$ and $Ce^{3+}$ [21–23], were also previously studied [24–28]. An in-depth analysis of these studies is desirable.

Lithium niobate ($LiNbO_3$) is a ferroelectric material which does not occur naturally. Due to its physical and chemical properties $LiNbO_3$ is an important material for many applications [29,30]. $LiNbO_3$ crystal is of sustained scientific and technical interest, mainly due to its desirable ferroelectric, piezoelectric, and photoelectric properties [31,32], even for acoustical memory as recently reported [31]. The most extensive application is the ferroelectric property which mainly origins from the structure distortion in $LiNbO_3$ itself, i.e. the $Li^+$ and $Nb^{5+}$ cations move away from their position in the paraelectric phase [33].

However, the reported values of the spin-Hamiltonian (SH) parameters obtained from EPR of $Fe^{3+}$ in $LiNbO_3$ are not uniform because of different experimental conditions and crystal composition [34–36]. It is necessary to systematize and complement previous studies.

Germanosillenite $Bi_{12}GeO_{20}$ (BGO) as well as $Bi_{12}SiO_{20}$ (BSO) crystals have been widely used in photorefractive, photoconductive, electro-optical and acousto-optical applications including two-wave mixing, four-wave mixing, phase conjugation, real-time holography, optical data storage, optical computing, electro-optical modulation, thin film optical waveguides [37–40].

Optical and photochromic properties of BGO:Cr crystals were early connected with chromium ions located in the $Ge^{4+}$ tetrahedral positions [41,42]. The chromium ions in BGO:Cr can be in $Cr^{4+}$ and $Cr^{5+}$ state [41,42]. The EPR spectra of Cr ions in BGO crystals were also previously studied [43] and in-depth analysis of these studies is desirable also.

Rare earth (RE) doped gadolinium calcium oxoborate $Ca_4GdO(BO_3)_3$ (GdCOB) crystals attract significant interest of researchers, since they are promising materials for bi-functional lasers and non-linear optical transformations [44,45]. Their possible applications are: colour displays, data storage devices, medical diagnostic, quantum electronics and optoelectronic materials. A possibility of effective doping the GdCOB crystal by different RE ions was demonstrated in Refs. 46,47. Incorporation of RE elements leads to an enhancement of the non-linear optical coefficient, improvement of emission efficiency, phase matching and technological conditions. EPR study of these centres are promising and important.

The aim of this review paper is to complete characteristics of impurities presented in selected oxide crystals as indicated by EPR measurements. For this purpose, the spin Hamiltonian analysis of EPR spectra has been carried out on the basis of the triclinic ($C_i$) site symmetry. Comparison of examined defects in different crystals enable us to find optimal conditions in order to improve the properties of the laser materials.

## 2. Crystal structure of invstigated materials

The crystal structure of materials studied by EPR is critical for in-depth analysis of experimental data. There are also the exact characteristics required in the first place.

### 2.1. Yttrium orthoaluminate crystals

The structural data indicate that YAP crystallizes in an orthorhombically distorted perovskite structure with the lattice parameters a = 0.518 nm, b = 0.533 nm, c = 0.737 nm [4,48,49]. The space group $D_{2h}^{16}$ was chosen to describe the symmetry of the unit cell in YAP crystals using the Pbnm group coordinate system [48,49]. The structure of $YAlO_3$ can be represented (see Fig. 1) as a grid of tilted $AlO_6$ octahedra with the Y ions occupying the empty space between the octahedra. The ionic radii of the cations, R, are $R(Y^{3+}) = 0.097$ nm, $R(Al^{3+}) = 0.057$ nm, $R(Co^{3+}) = 0.064$ nm, $R(Co^{2+}) = 0.078$ nm, $R(Nd^{3+}) = 0.099$ nm and $R(Er^{3+}) = 0.085$ nm [50]. The O–Al–O angles in the respective octahedra vary in the range 89.6°–90.6°.

Since deviations of the respective angles from 90° and the bond-length distortion are small, the $AlO_6$ octahedra may be considered to be only slightly distorted. The immediate surrounding of the Y cations consists of eight oxygen anions, whereas the Y—O bond-lengths in the $YO_8$ dodecahedra differ one from another, e.g. in the range from 0.2284 to 0.2597 nm for YAP–1% Nd. Hence, the $YO_8$ dodecahedra are considerably distorted with a bond-length distortion equal to 0.315 nm [4].

### 2.2. Lithium niobate

At room temperature, the space group in the ferroelectric phase is R3c with the hexagonal unit cell of $a_H = 0.515$ nm and $c_H = 1.386$ nm (Fig. 2). Below Tc (=1145 °C) the $C_3$ symmetry is characterized by a displacement of the cations ($Li^+$ and $Nb^{5+}$) along the crystallographic c-axis [51,52].

Due to the displacement of the cations, both ions reside in oxygen octahedra with small distortion. The stacking order of the octahedral sites along the c-axis becomes Li, Nb, structural vacancy (Vs), Li, Nb, Vs and so on. In the paraelectric phase, the point group of the material is $C_{3V}$ [51,52]. The oxygen layers are equally spaced along the c-axis. For the $Li^+$, $Nb^{5+}$ and $Fe^{3+}$ ions, the electro-

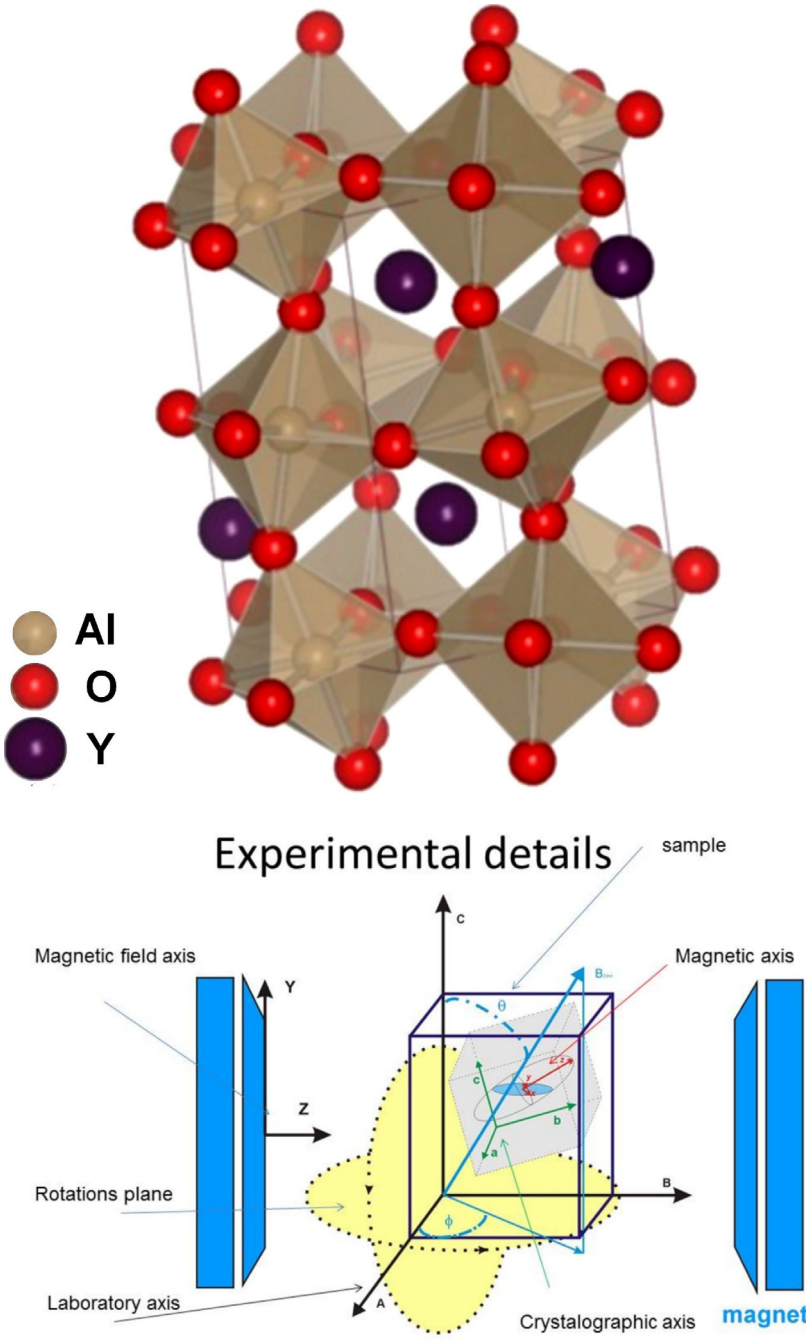


**Fig. 1.** The unit cell of $YAlO_3$ crystal and orientations of the sample for measurement.(YAP structure of the [27]).

negativities are 0.95, 1.7 and 1.8 and the ionic radii are 0.068, 0.069 and 0.064 nm, respectively.

### 2.3. Germanosillenite

In the germanosillenite ($Bi_{12}GeO_{20}$) structure presented in Fig. 3 (sp. gr. I23, lattice parameter a = 10.145 Å). The $GeO_4$ tetrahedra occupy the cube centre and vertices (the Ge–O distance is 1.717 Å) and $BiO_5$ polyhedra are located in the gaps between tetrahedra (the average Bi–O distance is 2.357 Å) [53]. The octahedron of oxygens around the Bi is strongly distorted.

Bismuth germinate, $Bi_4Ge_3O_{12}$, is a cubic crystal (space group 34) of the eulytine-type structure, with four formula units per unit cell (Fig. 4) The $Bi^{3+}$ site is coordinated by a distorted octahedron of six oxygen ions.

Each Ge ion is surrounded by four equivalent O ions to form $(GeO_4)_4-$ tetrahedra. The optical and photochromic properties of BGO:Cr crystals were due to the chromium ions located in the $Ge^{4+}$ tetrahedral positions and may occur both in $Cr^{4+}$ and $Cr^{5+}$ states [54].

### 2.4. Gadolinium calcium oxoborate

Gadolinium calcium oxoborate GdCOB crystal is biaxial what means that the optical axis (XY,Z) is not in coincidence with the crystallographic axis (a, b, c) [55,56].

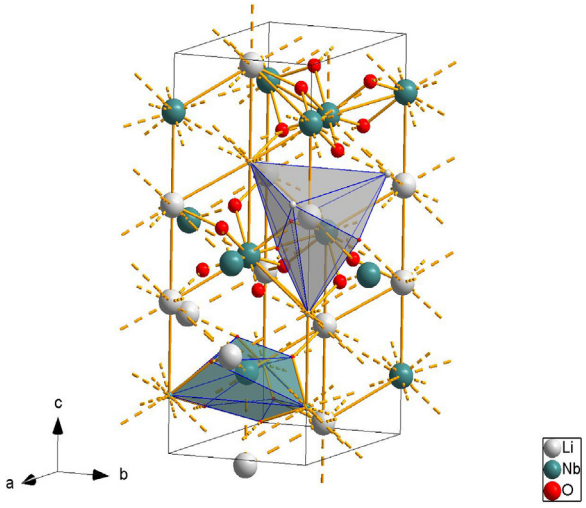


**Fig. 2.** The unit cell of Lithium niobate crystal.

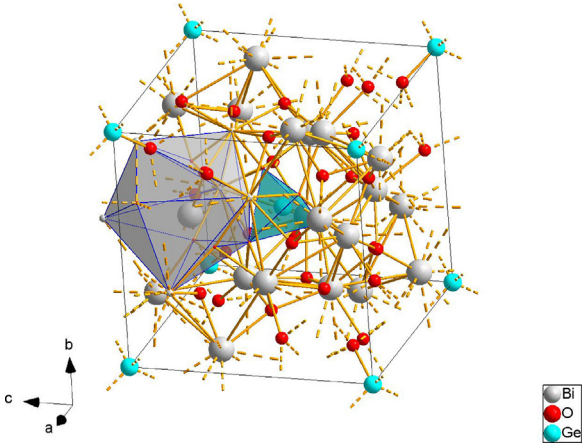


**Fig. 3.** The unit cell of Germanosillenite $Bi_{12}GeO_{20}$ crystal.

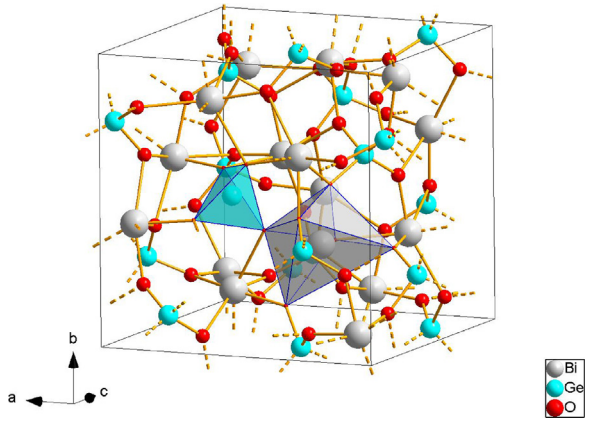


**Fig. 4.** The unit cell of Bismuth germinate, $Bi_4Ge_3O_{12}$ crystal.

GdCOB crystallizes in the monoclinic noncentrosymetric structure with two molecules per unit cell and space group symmetry Cm. The values of the unit cell constants are a = 0.8078 nm, b = 1.5981 nm, c = 0.35519 nm, and $\beta = 101.26^\circ$ [57]. GdCOB is isostructural to the calcium fluoroborate $Ca_5(BO_3)_3F$ [58].

There are two non-equivalent positions for $Ca^{2+}$ ion that occupy distorted octahedral sites. The crystal structure consists of $BO_3$ triangles and one oxygen ion O (1) which is free from boron. The two kinds of boron site, B(1) and B(2), with threefold coordination have a place. The planar borate unit lies approximately parallel to the (001) plane. The $Gd^{3+}$ ions are located in the crystallographic mirror plane (Fig. 5). The environment of $Gd^{3+}$ ion is a distorted octahedron with Cs site symmetry. Four oxygen ions are shared with the $BO_3$ groups. The existence of a probable disorder between calcium and gadolinium atoms in the two octahedral positions is expected [59,60].

## 3. EPR spectra: experimental details and results

### 3.1. General

The crystals investigated were grown in the Military University of Technology and in the Institute of Physics, Polish Academy of Sciences by the Czochralski technique using platinum crucible.

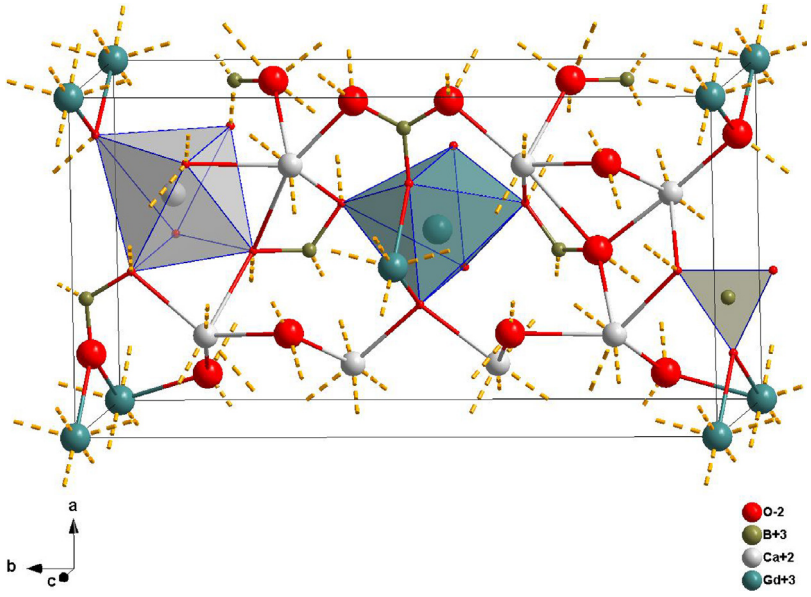


**Fig. 5.** Crystal structure of GdCOB.

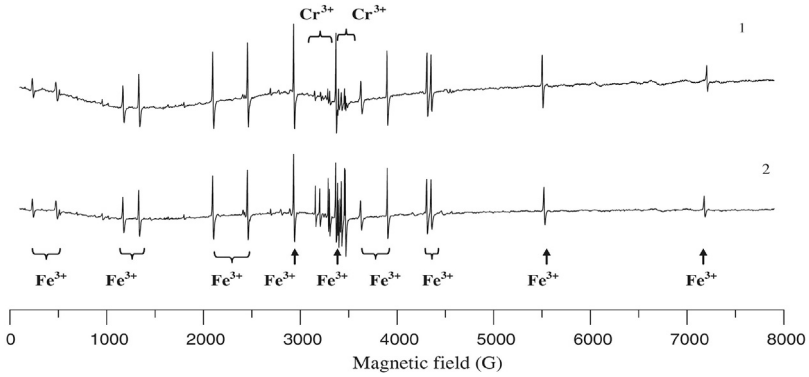


**Fig. 6.** EPR spectra of $Fe^{3+}$ and $Cr^{3+}$ ions in the as-grown crystals 1 and the $H_2$ annealed crystals 2. Lines corresponding to $Cr^{3+}$ and $Fe^{3+}$ ions are marked by arrows [24].

Some samples of the YAP as-grown crystals were annealed in $N_2 + H_2$ atmosphere (1100 and 1500 K) and in air (1400 K), as well as were irradiated with g-quanta from a $^{60}Co$ source up to $10^6$ Gy absorbed doses and with continuous and pulsed Ar+-laser light (l = 351 nm) of 1 W power.

One sample was irradiated by $^{235}U$ ions with energy 9.47 MeV/u (the total particle's energy was 2225 MeV) and fluency $5 \times 10^{11} cm^{-2}$ at room temperature, without control of temperature and without cooling (Institute for Heavy Ion Research at Darmstadt). Because BGO:Cr crystal exhibit strong photochromic effect, our sample was protected during irradiation by Al foil (thickness of 5 μm). This foil reduces of the particles' energy to 2120 MeV. irradiation by bismuth ions with energy 11.4 MeV/u (MeV per nucleon) and a fluence $5.10^{11}$ $cm^{-2}$ at room temperature. A detailed description of the methodology of measurement is presented in Refs. 25–28.

EPR spectra in a wide range of temperatures from 5 K to 300 K using an EPR X-band spectrometer (Bruker multifrequency and multiresonance FT-EPR ELEXSYS E580) were investigated. The angular dependences of EPR spectra were studied using a one-degree goniometer. Quantitative analysis of EPR spectra has been carried out using the program EMR_NMR [61] assuming spin Hamiltonian for a triclinic site symmetry. In this paper an extension of the computer program Superposition Model-Monte Carlo (SPM-MC) [62,63] designed for modelling of the spectroscopic and structural properties of transition ions at low symmetry sites in crystals was used. The predicted the zero-field splitting (ZFS) parameters obtained based on an SPM confirm correlation between the ZFS parameters obtained from experimental EMR spectra and structural data. The estimation of the spin-lattice relaxation time $T_1$ can be madeusing the conventional theory of the EPR line broadening.

Analysis of EMR spectra was performed using spin Hamiltonian (SH) suitable for transition ions [64]. For arbitrary low (triclinic) symmetry SH [65,66] is best expressed in terms of the extended Stevens operators (ESO) $O_k^q$ [67,68]:

$$H_s = \mu_B B \cdot g \cdot S + \sum B_k^q O_k^q(S_X, S_Y, S_Z)$$
$$= \mu_B B \cdot g \cdot S + \Sigma f_k b_k{}^q O_k{}^q \quad (1)$$

where $\boldsymbol{g}$ represent the Zeeman electronic tensor, $\boldsymbol{B}$ is the external magnetic field, $S_i$ are the spin operators, and $B_k^q$ ($b_k^q$) are the zero-field splitting parameters (ZFSPs). The 'scaling' factors $f_k$ in Eq. (1) are most commonly defined as [65,66]: $f_2 = 1/3$; $f_4 = 1/60$; $f_6 = 1/1260$. For proper relations between the conventional ZFSPs and $B_k^q$ ($b_k^q$) in Eq. (1), see [65,66,69]. For $Cr^{3+}$ (S = 3/2) ions only the ZFSPs with $k = 2$ are required, whereas for $Fe^{3+}$ (S = 5/2) ions – with $k = 2$ and 4.

A superposition model [69–72] represents the ZFSPs as linear combinations of products of the intrinsic parameters ($\bar{b}_k$), depending on the kind of ligands and their distances from the central ion, and the coordination factors ($K_k^q$), depending on the angular positions of ligands.

Full listing of the $K_k^q$ factors obtained using transformation properties of ESOs for arbitrary symmetry and $k = 2$, 4, and 6 may be found in Ref. 72. SPM calculations for the 2nd-rank ZFSPs may be carried out in two ways as described for $Cr^{3+}$ and $Fe^{3+}$ ions in YAP in [62,63].

### 3.2. Yttrium orthoaluminate crystals

Analysis of EPR spectra enables assignment of specific lines to various paramagnetic centres as follows. The two distinct groups of EPR lines observed in YAP:Fe,Cr crystals were identified as due to $Fe^{3+}$ and $Cr^{3+}$ ions (see Fig. 6) [24].

A decrease in the line intensity for $Fe^{3+}$ ions and a simultaneous increase for $Cr^{3+}$ ions is observed in the annealed crystals. The changes of the $Fe^{3+}$ and $Cr^{3+}$ line intensity indicate that recharging processes $Fe^{3+} + e^- \rightarrow Fe^{2+}$ and $Cr^{4+} + e^- \rightarrow Cr^{3+}$ occur in the reduced crystals [24]. EPR spectra of $Co^{2+}$ ions in YAP are only observed at temperatures below 30 K. Such EPR spectrum is presented in Fig. 7. Analysis of the experimental angular dependences reveals the existence of two different types of $Co^{2+}$ complexes, labelled α and β, both with an effective spin S = 1/2. The α-complex spectra exhibit a visible strong hyperfine structure.

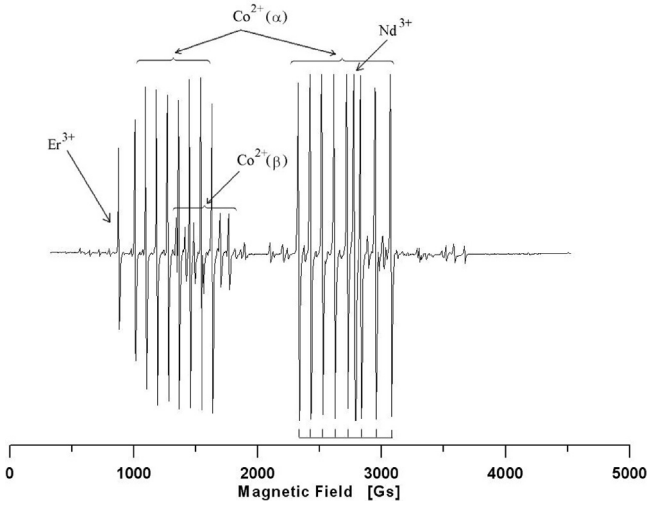


**Fig. 7.** EPR spectra of $Co^{2+}$ ions in YAP:Co crystals at 12 K.

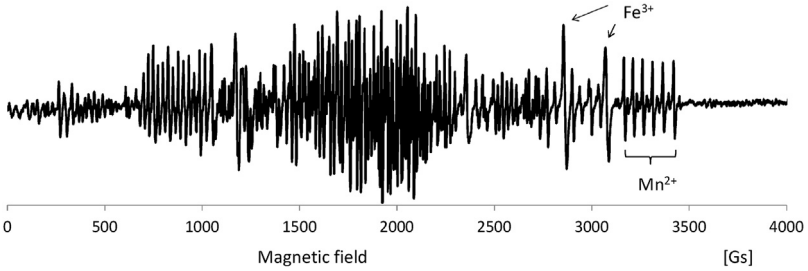


**Fig. 8.** EPR spectra of $Mn^{2+}$ ions in YAP:Mn crystals at room temperature. Selected lines corresponding to $Mn^{2+}$ and $Fe^{3+}$ ions are marked by arrows.

**Table 1**
Principal values (PVs) of the matrices g & D in the laboratory xyz axis system for $Fe^{3+}$, $Cr^{3+}$ $Co^{2+}$ (α), $Co^{2+}$(β), $Er^{3+}$ and $Nd^{3+}$ complexes in YAP crystals. The $A_i$ and $D_i$ values are in units of ($10^{-4}$ $cm^{-1}$).

| | $Fe^{3+}$ | $Cr^{3+}$ | $Co^{2+}$ (α) | $Co^{2+}$ (β) | $Er^{3+}$ | $Nd^{3+}$ |
|---|---|---|---|---|---|---|
| $g_x$ | 2.180 | 2.029 | 5.42(1) | 6.67(1) | 8.925(4) | 2.799(4) |
| $g_y$ | 2.065 | 2.012 | 5.02(1) | 3.70(1) | 8.038(3) | 2.539(3) |
| $g_z$ | 1.479 | 1.921 | 1.13(1) | 1.81(1) | 2.896(2) | 1.713(2) |
| $D_x$ | 512.1 | 324.3 | – | – | – | – |
| $D_y$ | -41.0 | -26.0 | – | – | – | – |
| $D_z$ | -471.0 | -298.0 | – | – | – | – |
| $A_x$ | – | – | 288(1) | 178(1) | 312(10) | 273(10) |
| $A_y$ | – | – | 164(1) | 84(1) | 311(10) | 228(10) |
| $A_z$ | – | – | 82(1) | −8.7(5) | 230(10) | 215(10) |
| Reference | [27] | [27,62] | [26] | [26] | [26] | [25] |

**Table 2**
The positions of the oxygen ligands (i = 1 ÷ 6) in the $MO_6$ octahedra in the polar coordinates.

| Ligand's number *i*: | | 1 | 2 | 3 | 4 | 5 | 6 |
|---|---|---|---|---|---|---|---|
| $AlO_6$ [18] | $R_i$ [nm] | 0.1901 | 0.1901 | 0.1910 | 0.1910 | 0.1921 | 0.1921 |
| | $\theta_i$ [°] | 14.2 | 165.8 | 80.2 | 99.8 | 80.2 | 99.8 |
| | $\phi_i$ [°] | 196.7 | 16.7 | 56.0 | 236.0 | 324.4 | 144.4 |
| $FeO_6$ | $R_i$ [nm] | 0.243 | 0.256 | 0.239 | 0.26 | 0.235 | 0.266 |
| | $\theta_i$ [°] | 87.51 | 92.47 | 85.61 | 92.15 | 2.664 | 175.5 |
| | $\phi_i$ [°] | 2.646 | 181.6 | 91.69 | 267.8 | -1.949 | 181.3 |
| $CrO_6$ | $R_i$ [nm] | 0.2010 | 0.1967 | 0.2041 | 0.2033 | 0.2088 | 0.2162 |
| | $\theta_i$ [°] | 16.3 | 86.5 | 88.1 | 101.2 | 175.6 | 100.1 |
| | $\phi_i$ [°] | 205.1 | 57.2 | 331.7 | 241.6 | 22.0 | 154.1 |

Four sets of lines due to the transitions between the lowest Kramers doublet levels with Ms = ±1/2 were observed.

The analysis of the angular dependences of the β-type spectra and the crystallographic data suggests that the Co(β) ions occupy two equivalent positions in the unit cell. Hence, the β complex can be tentatively attributed to $Co^{2+}$ ions located at the $Y^{3+}$ sites with $C_s$ local site symmetry. Analysis of the EPR spectra and the fittings will be performed assuming the local site symmetry $C_i$ in case of the $Co^{2+}$ (α) complex, as well as the $Co^{2+}$ (β) complex in case of $C_s$ and $Er^{3+}$, $Nd^{3+}$ ions as will be shown below (see also Refs. 25,26,27).

Analysis of EPR spectra in YAP:Mn crystals (Fig. 8) enables to assign specific lines to various paramagnetic centres as follows. Two distinct groups of EPR lines observed (see Fig. 8) were identified as due to $Fe^{3+}$ and $Cr^{3+}$ ions. Thus, the angular variations of EPR spectra for $Fe^{3+}$ and $Cr^{3+}$ ions are similar to those presented in our earlier paper [27].

For analysis and fitting, the sets of lines that correspond to a specific magnetically inequivalent position out of four for each ion-complex were selected. This selection was made on the basis of a comparison of the present spectra with those in Refs. 19,73 which allowed for two choices of lines in a given plane. Subsequently, theoretical simulations of the lines have been done using the program EMR_NMR version 6.51 [61] in order to verify correctness of our selections.

Four sets of lines were observed for each type of ions, which occupy four equivalent (crystallographically) but magnetically inequivalent positions in the YAP unit cell, which consists of four aluminium-oxygen pseudo-cells each with a different orientation with respect to the crystallographic axes. The next group of EPR spectra is assigned to a manganese ion. Four sets of lines of 150–600 mT were observed for $Mn^{4+}$ ions, which occupy four crystallographically equivalent but magnetically inequivalent positions in the YAP unit cell.

The next group of EPR lines of 250–400 mT is assigned to the $Mn^{2+}$ ion also and takes two crystallographically equivalent but magnetically inequivalent positions in the YAP unit cell. Principal values (PVs) of the matrices g and D in the laboratory xyz axis system for $Fe^{3+}$, $Cr^{3+}$ $Co^{2+}$ (α), $Co^{2+}$(β), $Er^{3+}$ and $Nd^{3+}$ complexes in YAP crystals (with different dopand) are presented in Table 1.

The EPR spectra of YAP crystals, nominally pure and doped with $Co^{2+}$ ions, as well as their analysis confirm the existence of paramagnetic $Cr^{3+}$ and $Fe^{3+}$ centres which occupy four magnetically inequivalent aluminum positions in the unit cell with the octahedral coordination exhibiting triclinic site symmetry. For $Fe^{3+}$ ions the fourth-rank ZFSPs were also obtained and presented in our paper [27].

Using the ZFS parameters and the pertinent conversion relations derived by authors of Refs. 27,70 the program SPM-MC computes feasible positions of the oxygen ligands in a given unit cell volume that yield the SPM-predicted ZFSPs consistent with the experimental ZFSPs.

Numerical calculations and analysis were carried out for the $FeO_6$ and $CrO_6$ in $YAlO_3$ complexes. During calculations the angles $\theta_i$ and $\varphi_i$ were varied in the range of several degrees from the starting values reported for the undistorted $AlO_6$ octahedron, whereas the minimum distances $R_i$ were computed from the ionic radii. The averaged values ($\theta_i$, $\varphi_i$; $R_i$) obtained from the program SPM-MC are listed in Table 2 together with the crystallographic data for the $AlO_6$ octahedron in pure crystal.

Therefore, the SPM analysis enables prediction of the most probable model of distortions around $Fe^{3+}$ and $Cr^{3+}$ ions in $YAlO_3$. The predicted small radial distortions of the Fe(Al)$O_6$ complex correlate well with the size of the ionic radii of the dopant ions [62,63].

In summary, in the investigated YAP crystals were detected:

in nominally pure YAP crystals – unintentional impurities of $Cr^{3+}$ and $Fe^{3+}$

in the YAP: Co crystal – cobalt ($Co^{2+}$) and unintentional impurities $Cr^{3+}$, $Fe^{3+}$, $Er^{3+}$ and $Nd^{3+}$

in the YAP:Mn crystal–manganese ($Mn^{2+}$,$Mn^{4+}$) and unintentional impurities of $Cr^{3+}$ and $Fe^{3+}$

### 3.3. *Lithium niobate*

Selected EPR spectra of investigated LNO:Fe sample are presented in Fig. 9. For LNO:Fe sample after irradiations by bismuth ions the angular dependence in room temperature was obtained. Analysis of EPR spectra for LNO:Fe sample was performed using

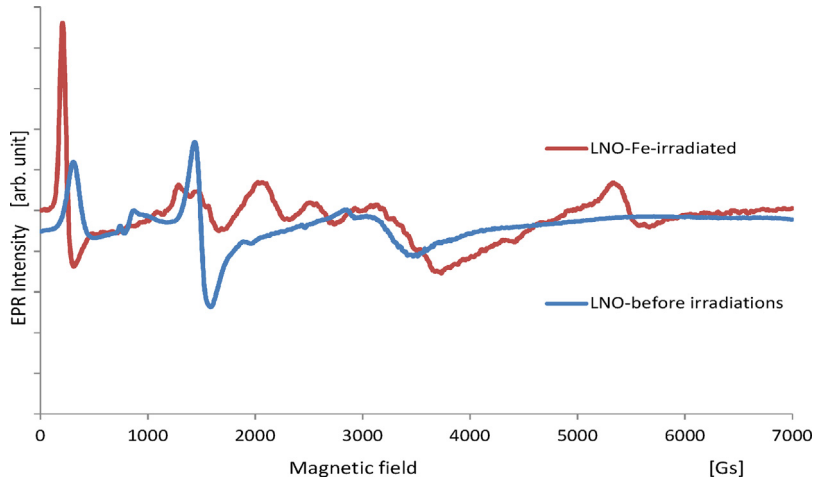


**Fig. 9.** Selected EPR spectra of LNO:Fe sample.

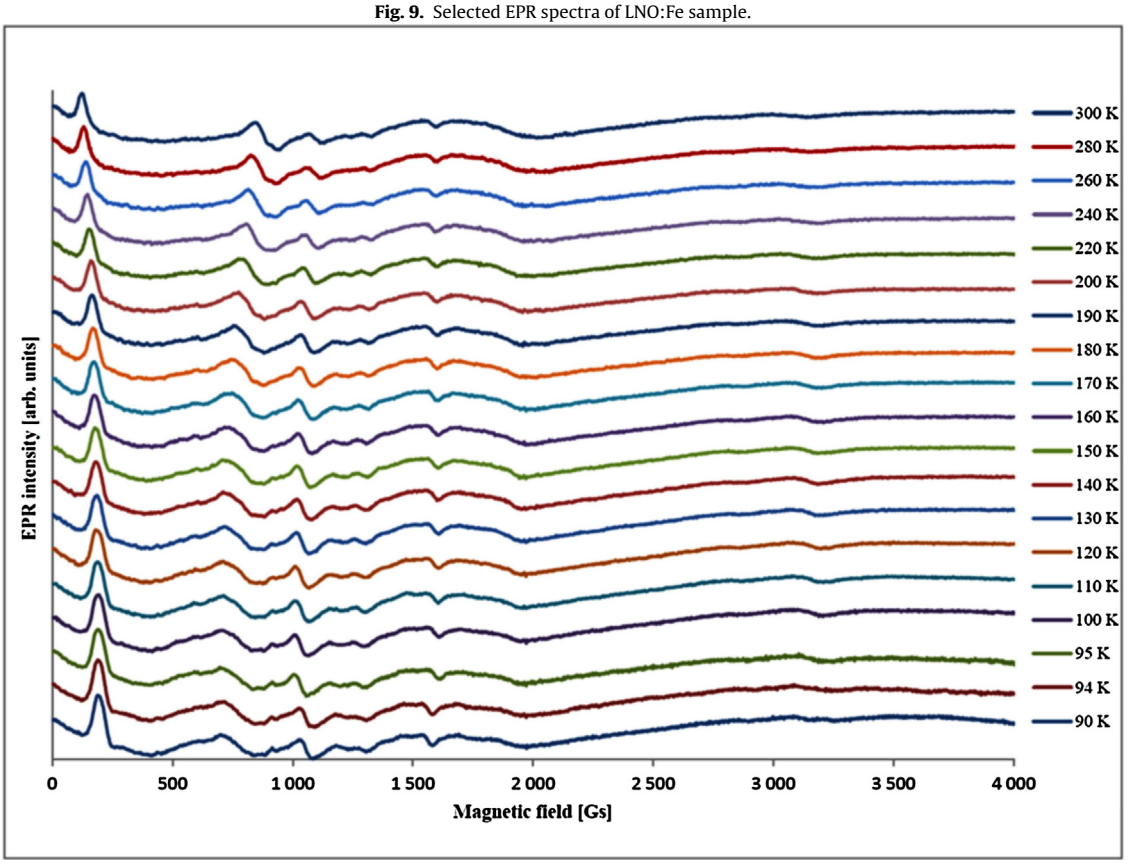


**Fig. 10.** Temperature dependence for LNO:Fe crystals.

standard spin Hamiltonians suitable for low spins at arbitrary low (triclinic) symmetry [Eq. (1)]. Temperature dependence (Fig. 10) was performed for after and before irradiation of LNO:Fe sample.

Temperature dependence of the EPR line of the peak-to-peak ($B_{pp}$) line widths were also measured. From these measurement the values of the broadening ($\Delta B$) of the EPR line width can be determined.

### 3.4. *Germanosillenite*

EPR spectra were measured for a non-irradiated sample, as well as for an irradiated sample (before and after annealing in air) in the temperature range of 140–370 K.

After measurements, the heating in air (time of heating was 20 min and temperature – 500 K) were performed by using an LHT 04/16 NABERTHERM furnace with a C42 controller. The EPR of investigated BGO:Cr samples are presented in Fig. 11.

For samples BGO-1 and BGO-2 temperature dependence of the $g_{eff}$ factor was determined (Table 3). Changes in $g_{eff}$ were observed after treatment, namely, for sample BGO-2 annealed after irradiation the change in the temperature dependence was stronger than for sample BGO-1 irradiated only.

After BGO:Cr irradiation, the fine structure of EPR spectra of chromium ions disappears. Irradiation of BGO:Cr crystals by uranium ions leads to the change of the structure of EPR spectra. Annealing of the irradiated sample leads to the changes of the line positions and creation of a new line in a higher magnetic field –

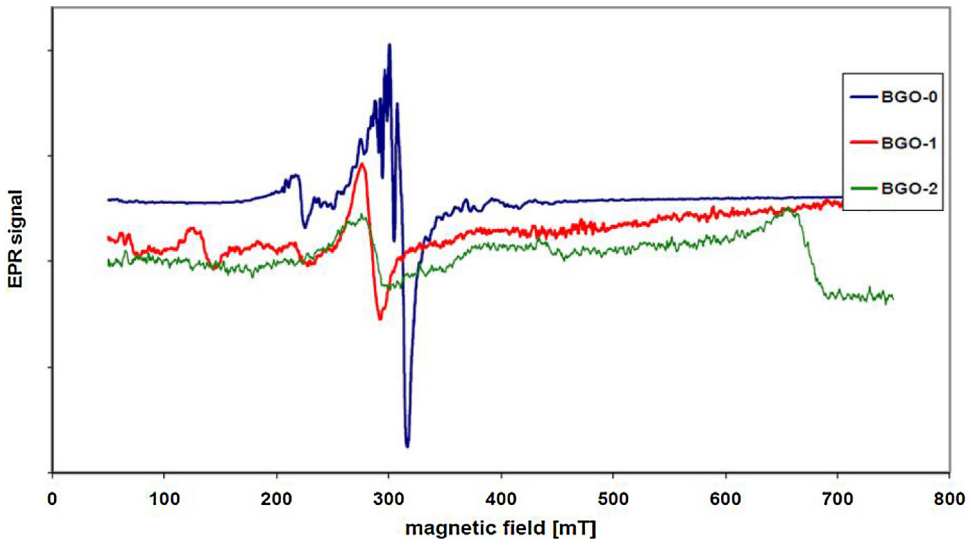


**Fig. 11.** EPR spectra of BGO-0- BGO:Cr crystal before uranium ions irradiation; BGO-1- BGO:Cr crystal after uranium ions irradiation; BGO-2– Sample BGO-1 after heating in air.

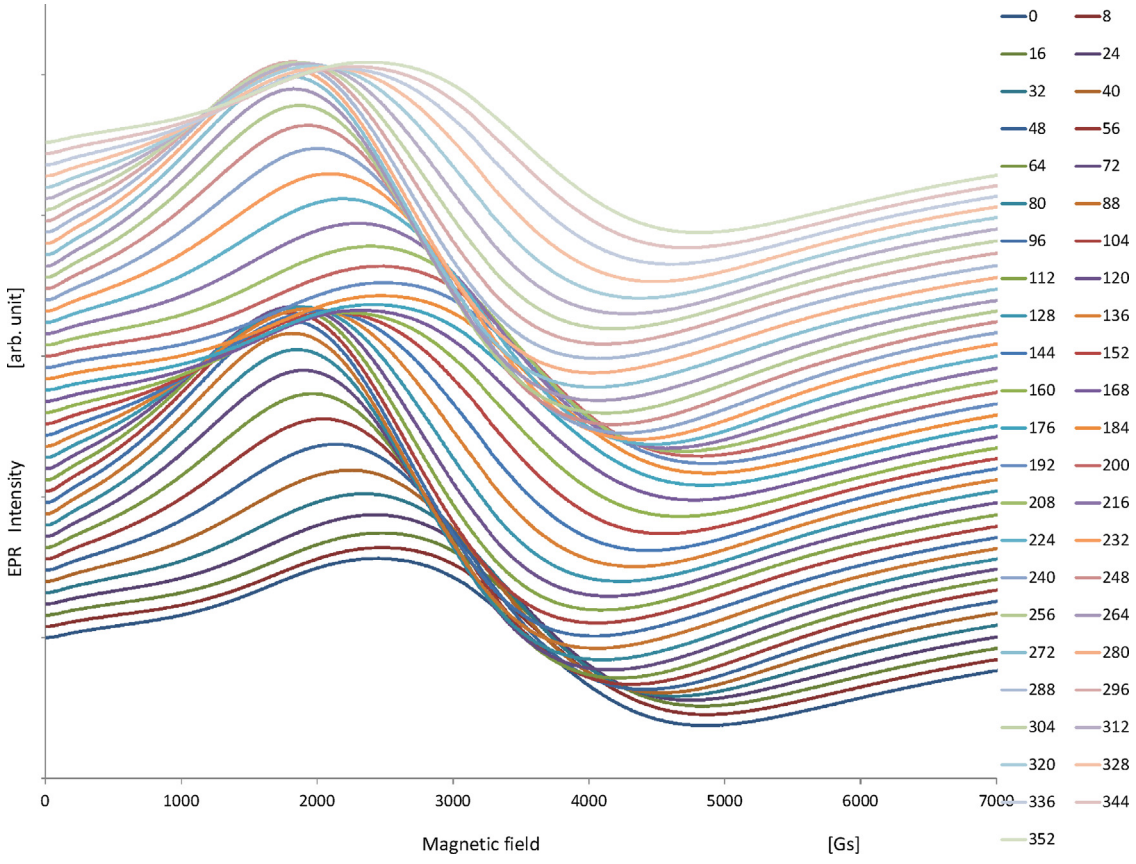


**Fig. 12.** Angular dependence of the EPR spectra of GdCOB crystal after irradiation by bismuth ions in room temperature.

**Table 3**
The spin Hamiltonian parameters determined from EPR spectra for the BGO crystals.

| Principal values | *Center-I* | *Center-II* | *Center-III* |
|---|---|---|---|
| $g_{xj}$ | 2.318 | 5.258 | 0.997 |
| $g_{yj}$ | 2.142 | 4.911 | 0.965 |
| $g_{zj}$ | 2.085 | 4.721 | 0.907 |
| References | [43] | [43] | This work |

center III, as it is shown in Fig. 11 and above presented analyses confirms.

### 3.5. *Gadolinium calcium oxoborate*

Measurements of the angular dependences of the EPR spectra were performed in three planes perpendicular to the crystallographic axes a, b and c. The selected EPR spectra are presented in Figs. 12 and 13.

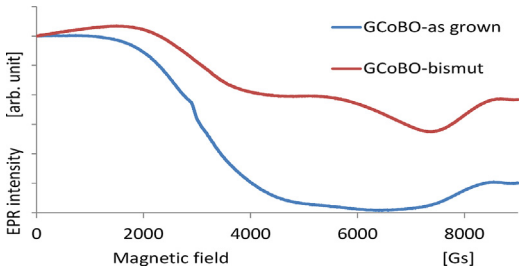


**Fig. 13.** EPR spectra of GdCOB crystal after and before irradiation by bismuth ions in room temperature.

**Table 4**
The spin Hamiltonian parameters determined from EPR spectra for the $Gd^{3+}$ complexes in GdCOB crystals.

| Principal values | as grown $Ca_4GdO(BO_3)_3$ | as grown $Ca_4GdO(BO_3)_3$ after irradiation |
|---|---|---|
| $g_{xj}$ | 2.806(5) | 2.687(9) |
| $g_{yj}$ | 1.857(5) | 2.193(9) |
| $g_{zj}$ | 1.361(7) | 1.048(10) |

The spin Hamiltonian parameters determined from EPR spectra for the $Gd^{3+}$ complexes in GdCOB crystals after and before irradiation are presented in Table 4.

As a result of the irradiation by bismuth ions of GdCOB crystal paramagnetic centre has a smaller distortion of g tensor.

## 4. Spin–lattice relaxation time

The estimation of the spin–lattice relaxation time $T_1$ can be made with the conventional method of line broadening [63] using the expression [15]:

$$T_1^{-1} = 2.8 \times 10^{10} \pi g \Delta B \quad (2)$$

In the temperature range 120–240 K the relaxation time $T_1$ is governed by the Orbach process [15,64]:

$$T_1^{-1} = A\left(\exp\left(\frac{\delta}{k_B T}\right) - 1\right)^{-1} \quad (3)$$

where δ represents the energy splitting between the ground $Gd^{3+}$ state and the first excited state, whereas A is the constant characteristics of the Orbach process (in $s^{-1}$).

Temperature dependence of the EPR line intensities and that of the peak-to-peak line widths were also measured. From these measurements, the values of the broadening (ΔB) of the EPR lines, i.e., the spin-phonon part of the EPR line width, can be determined.

Fig. 14 presents the experimental temperature dependence of $T_1$ for the $Fe^{3+}$ ion in LNO and a theoretical curve fitted using Eq. (3).

The spin-lattice relaxation time $T_1$ for all studied crystals is presented in Table 5. A $T^9$ Raman process dependence of $T_1^{-1}$ was not observed because of the dominance of the exponential term. The parameter δ [$cm^{-1}$] obtained by fitting the temperature dependence of $T_1^{-1}$ represents the energy splitting between the ground doublet (whose paramagnetic resonance we observe) and the first excited state.

## 5. Conclusions

The above presented results of EPR studies of laser crystals, as well as deep-analyses of these results using the spin Hamiltonian examination of EPR spectra have been carried out on the basis of the triclinic ($C_i$) site symmetry allowing to draw some important conclusions.

The $Co^{2+}(\alpha)$ and $Co^{2+}$ (β) ions are identified as occupying the $Al^{3+}$ and $Y^{3+}$ positions, respectively, in the unit YAP crystal cell.

The EPR spectra of YAP crystals, nominally pure and doped with $Co^{2+}$ ions, as well as their analysis confirm the existence of paramagnetic $Cr^{3+}$ and $Fe^{3+}$ centres, which occupy four magnetically inequivalent aluminum positions in the unit cell with the octahedral coordination exhibiting triclinic site symmetry.

The principal values of the tensors g, D and A, as well as the orientation of their principal axes are also determined w.r.t. the

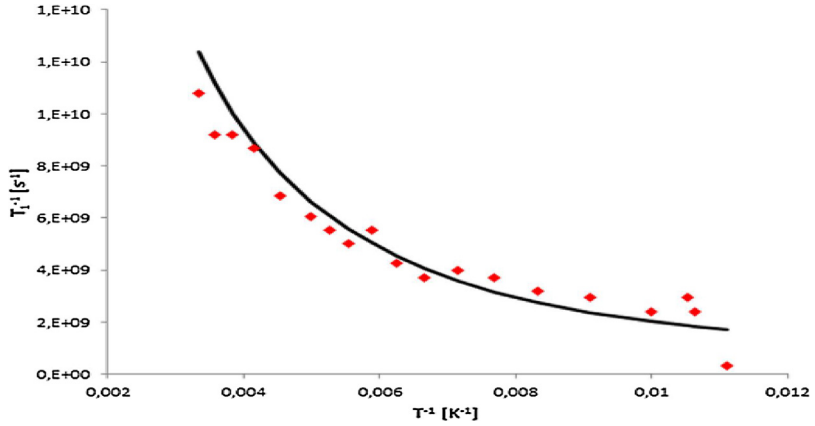


**Fig. 14.** Temperature dependence of the spin-lattice relaxation time $T_1$ for $Fe^{3+}$ ions in LNO crystal; the solid line represents an exponential fit using Eq. (2) with $A = 12 \times 10^{10}\ s^{-1}$, and $\delta = 208\ cm^{-1}$.

**Table 5**
The spin-lattice relaxation time $T_1$.

| | $Mn^{4+}$ ions in YAP | $Er^{3+}$ ions in YAP | $Nd^{3+}$ ions in YAP | $Fe^{3+}$ ions in LNO | B-center BGO-1 | B-center BGO-2 | C-center BGO-2 |
|---|---|---|---|---|---|---|---|
| δ [$cm^{-1}$] | 70 | 154 | 86 | 208 | 175 | 195 | 65 |
| $A*10^{10}$[$s^{-1}$] | 12 | 22 | 266 | 12 | 27 | 45 | 85 |
| References | [28] | [26] | [25] | This work | This work | This work | This work |

crystallographic axis system. Comparison of the directions of the local magnetic axes with the bond directions in the crystal structure shows a good agreement. Preliminary superposition model analysis yields the most probable models of distortions around the impurity $Cr^{3+}$ and $Fe^{3+}$ ions occupying the aluminum positions, which indicate small radial distortions of the Al-octahedra. This finding correlates well with the size of the ionic radii of the dopant ions.

The EPR spectra of YAP crystals doped with $Mn^{4+}$ ions, as well as their analysis confirm the existence of paramagnetic $Mn^{4+}$ centers which occupy four magnetically inequivalent aluminum positions in the unit cell with the octahedral coordination exhibiting triclinic site symmetry and $Mn^{2+}$ centres which occupy two magnetically inequivalent yttrium positions in the unit cell

The calculated spin-lattice relaxation times $T_1$ for $Fe^{3+}$ ions in the LNO and B-center in BGO crystals have similar values.

The complicated structure of the EPR spectra of the LNO:Fe indicates the presence of various paramagnetic centres after irradiations.

After irradiation of BGO:Cr, the fine structure of EPR spectra of chromium ions disappears. Irradiation of BGO:Cr crystals by uranium ions leads to the change of the structure of EPR spectra. The annealing of the irradiated sample leads to the changes of the line positions and creation of a new line in higher magnetic field.

For all of the irradiated by bismuth or uranium ions crystals radiation defects were observed, what does not generate point defects in the nearest neighbourhood of the paramagnetic ion. The best evidence is GdCOB crystal where the decrease in octahedral distortion in the environment of $Gd^{3+}$ ion is observed.

## References

[1] G.B. Loutts, M. Warren, L. Taylor, R.R. Rakhimov, H.R. Ries, G. Miller, M.A. Noginov, M. Curley, N. Noginova, N. Kukhtarev, H.J. Caulfield, P. Venkateswarlu, Manganese-doped yttrium orthoaluminate: a potential material for halographic recording and data storage, Phys. Rev. B 57 (7) (1998) 3706–3709.
[2] Ya. Zhydachevskii, A. Durygin, A. Suchocki, A. Matkovskii, D. Sugak, G.B. Loutts, M.A. Noginov, Radiation and thermally induced effects in YAlO3:Mn crystals, J. Lumin. 109 (1) (2004) 39–49.
[3] R.R. Rakhimov, A.L. Wilkerson, G.B. Loutts, M.A. Noginov, N. Noginova, W. Lindsay, H.R. Ries, Spin and valence states of manganese ions in manganese-doped yttrium orthoaluminate, Solid State Commun. 108 (8) (1998) 549–554.
[4] L. Vasylechko, A. Matkovskii, D. Savytski, A. Suchocki, F. Wallrafen, Crystal structure of GdFeO3-type rare earth gallates and aluminates, J. Alloys Compd. 291 (1–2) (1999) 57–65.
[5] M.A. Noginov, G.B. Loutts, Spectroscopic studies of Mn4+ ions in yttrium orthoaluminate, J. Opt. Soc. Am. B 16 (1) (1999) 3–11.
[6] M.A. Noginov, G.B. Loutts, M. Warren, Spectroscopic studies of Mn3+ and Mn2+ ions in YAlO3, J. Opt. Soc. Am. B 16 (3) (1999) 475–483.
[7] Ya. Zhydachevskii, A. Durygin, A. Suchocki, A. Matkovskii, D. Sugak, P. Bilski, S. Warchol, Mn-doped YAlO3 crystal: a new potential TLD phosphor, Nuclear Inst. Methods Phys. Res. B 227 (4) (2005) 545–550.
[8] I.F. Elder, M.J. Payne, Lasing in diode-pumped Tm:YAP, Tm, Ho:YAP and Tm, Ho:YLF, Opt. Commun. 145 (1–6) (1998) 329–339.
[9] A.A. Kaminskii, Laser Crystals, Springer, Heidelberg, Berlin, 1990.
[10] A.J. Wojtowicz, J. Glodo, A. Lempicki, C. Brecher, Recombination and scintillation processes in YAlO3:Ce, J. Phys. Condens. Matter 10 (1998) 8401–8415.
[11] A. Senyshyn, L. Vasylechko, Low temperature crystal structure behaviour of complex yttrium aluminium oxides YAlO3 and Y3Al5O12, Acta Phys. Polon. A 124 (2) (2013) 329–335.
[12] Z. Mierczyk, Nonlinear Absorbers The investigation of Features, Technology and Selected Applications, WAT Press, Warsaw, 2000, in Polish.
[13] S. Gołab, Z. Mierczyk, W. Ryba-Romanowski, Investigation of nonlinear absorption of LaGaO3: Co Crystals near 1.5 μm, Phys. Status Solidia 179 (2) (2000) 463–468.
[14] K. Yumashev, I. Denisov, N. Posnov, P. Prokoshin, V. Mikhailov, Nonlinear absorption properties of Co2+:MgAl2O4 crystal, Appl. Phys. B 70 (2000) 179–184.
[15] P. Aleshevych, M. Berkowski, W. Ryba-Romanowski, H. Szymczak EPR and optical spectra of cobalt in SrLaAlO4, Phys. Status Solidi b 218 (2000) 521–526.
[16] M. Kaczmarek, M. Berkowski, J. Fink-Finowicki, M. Kwasny, M. Palczewska, S. Warchoł, Growth and Characterization of SrLaGO7 single crystals highly doped with Co, Prace ITME 56 (151) (2000) a3 (in Polish).
[17] M. Yamaga, H. Takeuchi, T.J. Han, B. Henderson, Electron paramagnetic resonance and optical spectra of Cr3+ –doped YAlO3, J. Phys. Condens. Matter 5 (1993) 8097–8104.
[18] R.F. Belt, J.R. Latore, R. Uhrin, EPR and optical study of Fe in Nd:YAlO3 laser crystals, Appl. Phys. Lett. 25 (1974) 218–220.
[19] M. Yamaga, T. Yosida, B. Henderson, K. O'Donnell, M. Date, Electro paramagnetic resonance and optical spectra of Ti3+-doped YAlO3, J. Phys. Condens. Matter 4 (1992) 7285–7294.
[20] R.R. Rakhimov, E.M. Jackson, D.E. Jones, G.B. Loutts, Low-field microwave response and electron paramagnetic resonance identification of valence states of manganese including octahedral Mn5+ in YAlO3 and CaYAlO4, J. Appl Phys. 95 (2004) 5653–5660.
[21] G.R. Asatryan, J. Rosa, EPR of Er3+, Nd3+, and Ce3+ ions in YAlO3 single crystals, Phys. Solid State 44 (2002) 864–869.
[22] G.R. Asatryan, J. Rosa, J.A. Mares, EPR studies of Er3+, Nd3+ and Ce3+ in YAlO3 single crystals, Solid State Commun. 104 (1997) 5–9.
[23] R. Jablonski, Z. Frukacz, Electron-spin-resonance study of Nd3+ and Er3+ ions in YAlO3, Acta Phys. Polon. A 90 (2) (1996) 339–343.
[24] D. Sugak, A. Matkovskii, D. Savytskii, A. Durygin, A. Suchocki, Y. Zhydachevskii, I. Solskii, I. Stefaniuk, F. Wallrafen, Growth and induced color centers in YAlO3-Nd single crystals, Phys. Stat. Sol. (a) 184 (No. 1) (2001) 239–250.
[25] I. Stefaniuk, W. Obermayr, M. Rozborska, A. Matkowski, M. Kuzma, EPR study of Nd3+ impurities in YAlO3 single crystals, Mol. Phys. Rep. 37 (2003) 127–131.
[26] I. Stefaniuk, A. Matkovskii, C. Rudowicz, A. Suchocki, Z. Wilamowski, T. Lukasiewicz, Z. Galazka, Electron paramagnetic resonance studies of cobalt and rare-earth impurity ions in YAlO3, J. Phys. Condens Matter 18 (2006) 4751–4761.
[27] I. Stefaniuk, C. Rudowicz, P. Gnutek, A. Suchocki, EPR study of Cr3+ and Fe3+ impurity ions in nominally pure and Co2+-doped YAlO3 single crystals, Appl. Magn. Reson. 36 (2–4) (2009) 371–380.
[28] I. Stefaniuk, I. Rogalska, A. Suchocki, M. Berkowski, B. Cieniek, P. Potera, Electron paramagnetic resonance studies of manganese and cobalt ions in YAlO3 crystals, Opt. Appl. XLIV (1) (2014) 113–121.
[29.] A. Rauber, in: E. Kaldis (Ed.), Chemistry and Physics of Lithium Niobate, Current Topics in Material Science, 1987, Amsterdam North Holland.
[30] F. Agullo-Lopez, J.M. Cabrera, Properties of Lithium Niobate, EMIS Data reviews Series No. 5 INSPEC, 1989, London.
[31] M.S. McPherson, I. Ostrovskii, M.A. Breazeale, Observation of acoustical memory in LiNbO3, Phys. Rev. B 89 (2002) 115506–115508.
[32] D.J. Keeble, M. Loyo-Menoyo, Electron paramagnetic resonance of Fe3+ in LiNbO3, Phys. Rev. B 71 (2005) 224111–224118.
[33] D. Xue, K. Kitamura, J. Wang, Atomic packing and octahedral linking model of lithiumniobate single crystals, Opt. Mater. 23 (2003) 399–402.
[34] G.I. Malovichko, V.G. Vrachev, O.F. Schirmer, B. Faust, New axial Fe3+ centres in stoichiometric lithium niobate crystals, J. Phys. Condens Matter 5 (1993) 3971–3976.
[35] T.H. Yeom, S.H. Choh, Y.M. Chang, C. Rudowicz, Experimental and theoretical investigation of spin-hamiltonian parameters for the low symmetry Fe3+ centre in LiNbO3, Phys. Status Solidi B 185 (1994) 409–415.
[36] V.G. Grachev, G.I. Malovichko, Determination of the point symmetry of defects in crystals exhibiting structural phase transitions, using the temperature dependencies of the EPR spectra. Impurities in LiNbO3, Sov. Phys Solid State 27 (1985) 686–689.
[37] H. Rajbenbach, J. Huignard, Self-induced coherent oscillations with photorefractive Bi12SiO20 amplifier, Opt. Lett. 10 (1985) 137–139.
[38] M. Miteva, N. Dushkina, M. Gospodinov, 'Nonstationary amplification of the holographic recording in doped BSO crystals: a base for photorefractive incoherent-to-coherent optical conversion', Appl. Opt. 34 (20) (1995) 4083–4085.
[39] A.I. Grachev, A.A. Kamshilin, O.V. Kobozev, V.V. Prokofiev, Origin of transient effects in two-wave mixing experiments in BSO crystals, Optics of Crystals, in: V.V. Shepelevich, N.N. Egorov (Eds.), Proc. SPIE 4358 (2001) 102–108.
[40] D. Kip, Photorefractive waveguides in oxide crystals: fabrication, properties and applications, Appl. Phys. B Lasers Opt. 67 (2) (1998) 131–150.
[41] J.S. McCullough, A.L. Harmon Bauer, C.A. Hunt, J.J. Martin, Photochromic response of bismuth germanium oxide doped with chromium, J. Appl Phys. 90 (12) (2001) 6017–6021.
[42] W. Wardzynski, H. Szymczak, K. Pataj, T. Łukasiewicz, J. Zmija, Light induced charge transfer processes in Cr doped Bi12GeO20 and Bi12SiO20 single crystals, J. Phys. Chem. Solids 43 (8) (1982) 767–769.
[43] I. Stefaniuk, P. Potera, I. Rogalska, D. Wróbel, EPR investigations of defects in Bi12GeO20:Cr single crystal irradiated by high energy uranium ions, Curr. Top. Biophys. 33 (Suppl. A) (2010) 231–235.
[44] G. Aka, F. Mougel, F. Auge, A. Kahn-Harari, D. Vivien, J.M. Benitez, F. Salin, D. Pelenc, F. Balembois, P. Georges, A. Brun, Overview of the laser and non-linear optical properties of calcium-gadolinium-oxo-borate Ca4GdO(BO3)3, J. Alloys Compd. 303–304 (2000) 401–408.
[45] M. Iwai, T. Kobayashi, H. Furuya, Y. Mori, T. Sasaki, Crystal Growth and optical characterization of rare-earth (Re) calcium oxyborate ReCa 4O(BO 3) 3 (Re = Y or Gd) as new nonlinear, Opt. Mater. Jpn. J. Appl. Phys. 36 (Part 2) (1997) L276.
[46] M.G. Brik, A. Majchrowski, I.V. Kityk, T. Łukasiewicz, M. Piasecki, Spectroscopy of Ca4GdO(BO3)3 (GdCOB): Pr3+ single crystals, J. Alloys Compd. 465 (1–2) (2008) 24–34.

[47] G. Dominiak-Dzik, W. Ryba-Romanowski, S. Golab, A. Pajaczkowska, Visible and infrared spectroscopy of Pr3+ and Tm3+ ions in lead borate glasses, J. Phys. Condens Matter 12 (2000) 5495–5505.
[48] S. Geller, E.A. Wood, Wood Crystallographic studies of perovskite-like compounds. I. Rare earth orthoferrites and YFeO3, YCrO3, YAlO3, Acta Crystallogr. 9 (1956) 563–568.
[49] R. Diehl, G. Brant, Crystal structure refinement of YAlO3, a promising laser material, Mater. Res Bull. 10 (1975) 85–90.
[50] Z. Bojarski, M. Gigla, K. Stroz, M. Surowiec, Crystallography, PWN, Warsaw, 2001, in Polish.
[51] S.C. Abrahams, J.M. Reddy, J.L. Bernstein, Ferroelectric lithium niobate. 3, 4 and 5. Single crystal X-ray diffraction study at 24 °C, J. Phys. Chem. Solids 27 (1966) 997–1012, 1013-1018, 1019-1026.
[52] A.M. Glass, Optical Spectra of Cr3+ impurity ions in ferroelectric LiNbO3 and LiTaO3, J. Chem. Phys. 50 (1969) 1501–1510.
[53] S.C. Abrachams, P.B. Jamieson, I.L. Bernstein, Crystal chirality and optical rotation sense in isomorphous Bi12SiO20 and Bi12GeO20, J. Chem. Phys. 30 (5) (1979) 293–295.
[54] I.V. Stepanova, N.G. Gorashchenko, K.A. Subbotin, V.A. Smirnov, Determination of the charge state of chromium in Cr:Bi 12 GeO 20 single crystals by spectral luminescence methods, J. Opt. Spectrosc. 107 (2009) 335–338.
[55] G. Aka, A. Kahn-Harari, F. Mougel, D. Vivien, F. Salin, P. Coquelin, P. Colin, D. Pelenc, J.P. Damelet, Linear- and nonlinear-optical properties of a new gadolinium calcium oxoborate crystal, Ca4GdO(BO3)3, J. Pt. Soc. Am. B14 (9) (1997) 2238–2247.
[56] P. Segonds, B. Boulanger, B. Menaert, J. Zaccaro, J.P. Salvestrini, M.D. Fontana, R. Moncorge, F. Poree, G. Gadret, J. Mangin, A. Brenier, G. Boulon, G. Aka, D. Pelenc, Optical characterizations of YCa4O(BO3)3and Nd: YCa4O(BO3)3 crystals, Opt. Mater. 29 (8) (2007) 975–982.
[57] F. Mougel, A. Kahn-Harari, G. Aka, D. Pelenc, Structural and thermal stability of Czochralski grown GdCOB oxoborate single crystals, J. Mater. Chem. 8 (1998) 1619–1623.
[58] L. Shirong, H. Qingzhen, Z. Yifan, J. Aidong, C. Chuangtian, Structure of calcium fluoroborate, Ca5(BO3)3F, Acta Crystallogr. Sect. C 45 (1989) 1861–1863.
[59] A.B. Ilyukhin, B.F. Dzhurinskii, Crystal structure of binary oxoborates LnCa4O(BO3)3, J. Russ. Inorg. Chem. 38 (1993) 847–850.
[60] A. Pajaczkowska, A. Klos, B. Hilczer, N. Menguy, A. Novosselov, 'Growth of GdCa4O(BO3)3 by the czochralski method and some structure properties', Cryst. Growth Des. 1 (5) (2001) 363–365.
[61] D.G. McGavin, M.Y. Mombourquette, J.A. Weil, Computer Program EPR–NMR version 6.5, Department of Chemistry, University of Saskatchewan, Canada, 2002), 2018.
[62] I. Stefaniuk, C. Rudowicz, Computer program SPM-MC and its applications in EMR studies of transition ions in crystals, Curr. Top. Biophys. 33 (Suppl. A) (2010) 217–220.
[63] I. Stefaniuk, C. Rudowicz, Computer program superposition model-Monte Carlo (SPM-MC) and its applications in EMR studies of transition ions at low symmetry sites Fe3+ doped YAP crystals, Nukleonika 58 (3) (2013) 397–400.
[64] A. Abragam, B. Bleaney, Electron Paramagnetic Resonance of Transition Ions, Clarendon Press, Oxford, 1970.
[65] C. Rudowicz, Concept of spin Hamiltonian, forms of zero-field splitting and electronic Zeeman Hamiltonians and relations between parameters used in EPR. A critical review, Magn. Res Rev. 13 (1987) 1–89, Erratum, ibidem 13: 335.
[66] C. Rudowicz, S.K. Misra, Spin-hamiltonian formalisms in Electron Magnetic Resonance (EMR) and related spectroscopies, Appl. Spect. Rev. 36 (2001) 11–63.
[67] C. Rudowicz, Transformation relations for the conventional Okq and normalized O'kq Stevens operator equivalents with k = 1 to 6 and $-k \leq q \leq +k$, J. Phys. C 18 (1985) 1415–1430, Erratum: ibidem C 18: 3837.
[68] C. Rudowicz, C.Y. Chung, The generalization of the extended Stevens operators to higher ranks and spins, and a systematic review of the tables of the tensor operators and their matrix elements, J. Phys. Condens. Matter 16 (2004) 5825–5847.
[69] C. Rudowicz, On the relations between the zero-field splitting parameters in the extended Stevens operator notation and the conventional ones used in EMR for orthorhombic and lower symmetry, J. Phys. Condens. Matter 12 (2000) L417–L423.
[70] D.J. Newman, W. Urban, Interpretation of S-state ion E. P. R. spectra, Adv. Phys. 24 (1975) 793–844.
[71] D.J. Newman, B. Ng, The superposition model of crystal fields, Rep. Prog. Phys. 52 (1989) 699–763.
[72] C. Rudowicz, On the derivation of the superposition model formulas using the transformation relations for the Stevens operators, J. Phys. C: Solid State Phys. 20 (1987) 6033–6037.
[73] R.L. White, G.F. Herrmann, J.W. Carson, M. Mandel, Paramagnetic Resonance of Fe3+ and Gd3+ in Yttrium Orthoaluminate, Phys. Rev. 136 (1A) (1964) 231–239.